

## RESEARCH ARTICLE

WILEY

# Evaluating the capability of a UAV-borne spectrometer for soil organic carbon mapping in bare croplands

He Zhang<sup>1</sup>  | Pu Shi<sup>1</sup> | Giacomo Crucil<sup>1</sup> | Bas van Wesemael<sup>1</sup> |  
 Quentin Limbourg<sup>2</sup> | Kristof Van Oost<sup>1</sup>

<sup>1</sup>Earth and Life Institute, Georges Lemaître Center for Earth and Climate Research, UCLouvain, Louvain-la-Neuve, Belgium

<sup>2</sup>Walloon Agricultural Research Centre (CRA-W), Farming Systems, Territories and Information Technology Unit, Gembloux, Belgium

## Correspondence

He Zhang, Earth and Life Institute, Georges Lemaître Center for Earth and Climate Research, UCLouvain, Louvain-la-Neuve 1348, Belgium.  
 Email: he.zhang@uclouvain.be

## Funding information

Belgian Federal Science Policy Office, Grant/Award Number: SR/00/362; China Scholarship Council, Grant/Award Number: 201706300034

## Abstract

High-resolution, field-scale soil organic carbon (SOC) mapping in croplands is crucial for effective and precise agricultural management. Recent developments in unmanned aerial vehicles (UAVs) combined with miniaturized visible–near infrared spectrometers have enabled the rapid and low-cost field-scale SOC mapping. However, a field-specific spectrotransfer model is often needed for such UAV-based hyperspectral measurements, implying local sampling and model development are still required, and this hampers the widespread application of UAV-based methods. In this study, we aim to test to what extent SOC prediction models derived from an existing regional soil spectral library (SSL) can be applied to UAV-based hyperspectral data, without the need for additional field sampling. To this end, an UAV survey was conducted over a bare cropland within the Belgian Loam Belt for field-scale SOC mapping. We evaluated two calibration approaches, one based on local sampling and model development, and one where we capitalized on an existing (laboratory-based) regional SSL. For the local calibration approach, we obtained a good prediction performance with RMSE of 0.57 g kg<sup>-1</sup> and RPIQ of 2.35. For the regional model, a spectral alignment procedure was needed to resolve the discrepancy between UAV- and laboratory-based measurements. This resulted in a fair SOC prediction accuracy with RMSE of 0.93 g kg<sup>-1</sup> and RPIQ of 1.45. The comparison of SOC maps derived from the two approaches, along with an external validation showed a high consistency, indicating that UAV-based spectral measurements, in combination with SSLs have the potential to improve the efficiency of high-resolution SOC mapping.

## KEYWORDS

hyperspectral sensors, precision agriculture, soil organic carbon, soil spectral library, UAV, Vis–NIR spectroscopy

## 1 | INTRODUCTION

Soil organic carbon (SOC) affects many soil properties and functions, including the ability to retain water and nutrients, to provide structure promoting efficient drainage and aeration and to reduce loss of topsoil via erosion (Ontl & Schulte, 2012; Robertson et al., 2014). SOC therefore plays a central role in the sustainable management of soil through

its control on soil productivity, carbon sequestration, water purification and retention, and soil biogeochemical cycling (Stockmann et al., 2013). Direct measurements of SOC are critical to assess current SOC contents and to inform the selection of appropriate management strategies where SOC contents are low. However, conventional methods of measuring and mapping soil carbon at field to landscape scales are usually labour-intensive due to the large number of samples

required to cover the spatial variability of soils (Miklos et al., 2010). Furthermore, monitoring changes in SOC in an efficient way and with sufficient statistical confidence (de Gruijter et al., 2016), remains challenging as assessments are largely influenced by the sampling design (Vašát et al., 2010).

In response to these demands, a broad range of spectroscopic methods have been developed and are now routinely used as fast and reliable tools for estimating SOC. SOC exhibits diagnostic absorption features within the visible–near infrared (VNIR: 400–1300 nm) and short-wave infrared (SWIR: 1300–2500 nm) spectral regions (Chabrilat et al., 2019; Goetz et al., 1985). Soil spectroscopy exploits the correlation between spectral features and chromophores for the quantitative determination of SOC concentration (Mohamed et al., 2018). More recently, the success of laboratory-based soil spectroscopy has been translated into proximal and remote sensing platforms for the estimation of SOC at large scale (e.g., Castaldi, Chabrilat, Jones, et al., 2018; Shi et al., 2020). Due to its high spatial resolution and small influence of atmospheric factors, close-range UAV-based spectroscopy has shown large potential to capture the field-scale variability of SOC and to aid better and more targeted agricultural management. UAV-based spectroscopy can be based on multispectral camera (Aldana-Jague et al., 2016; Biney et al., 2021) or hyperspectral imagery (Laamrani et al., 2019). However, at present these approaches require massive soil sampling efforts for the development of local spectroscopic prediction models, and this remains an important bottleneck (Aldana-Jague et al., 2016; Brown et al., 2005).

Along with the increasing availability of soil data, open-access soil spectral libraries (SSLs) have been developed and enable a data-driven approach to effectively provide soil information (Ballabio et al., 2016). Exploiting the SSL to derive spectroscopic prediction models for SOC estimation could alleviate the workload of local soil sampling and chemical analyses (e.g., Castaldi, Chabrilat, Chartin, et al., 2018; Guerrero et al., 2016). To exploit a model calibrated with library, however, it is necessary to keep the same protocol in the field and laboratory. Nevertheless, there exists a large discrepancy between soil spectra collected under optimal laboratory conditions and those acquired in situ via close-range UAV sensing, as data acquisition equipment, protocols, and soil conditions are very different. In this case, a spectral transfer procedure can be applied to quantify and correct the differences between the spectral outputs provided by the two instruments, commonly called master and slave instruments. Past work has relied on the concept of standard measurement protocols and internal soil standard (ISS) to align data acquired using diverse spectrometers and protocols under controlled laboratory conditions (Kopačková & Bendor, 2016). However, it remains unknown to what extent this approach can be adopted to align spectral data measured from different sources/platforms, for example, UAV-based spectra (outdoor condition, different spatial dimension) versus laboratory spectra (controlled indoor conditions), and to what extent the discrepancy can be corrected so as to apply the SSL-based model on UAV-based spectra for a field-scale SOC mapping.

We performed a case study consisting of UAV-based spectral measurement and SOC analysis in a cropland at the central part of the

Belgium Loess Belt. This study presents a workflow for acquiring hyperspectral information from close-range UAV-borne spectrometer and tests whether it can be used to accurately predict spatial patterns of SOC content at field scale. Furthermore, we integrate existing soil data and spectral archives into the workflow, so as to alleviate the effort needed for local sampling. We aim to implement and evaluate spectral alignment procedures so that spectral readings measured from different platforms/conditions (i.e., UAV- versus laboratory-based) can be integrated. The objectives of this study are to (i) evaluate the quality of hyperspectral measurements derived from a UAV-borne spectrometer and (ii) present and evaluate a workflow where a regional SLL is used to convert UAV-based spectral readings into SOC predictions. Finally, we discuss the capability of UAV-based spectrometer sensing for mapping SOC contents on bare croplands.

## 2 | MATERIAL AND METHODS

### 2.1 | Study area

The study area is located within the Belgian Loam Belt in the northern part of Wallonia. The area covers the central loess belt from Gembloux to Lincent (9.7 km-wide and 40 km-long, SW corner: 50.60 N, 4.65 E; NE corner: 50.70 N, 5.06 E) (Figure 1a). The main soil type in the area are Luvisols that are characterized by a silt loam texture and well-drained soils. The climate of the region is temperate oceanic with mean temperatures between 2.3°C (January) and 17.8°C (July) and a mean annual precipitation of 790 mm (RMI, <https://www.meteo.be>).

### 2.2 | Data collection

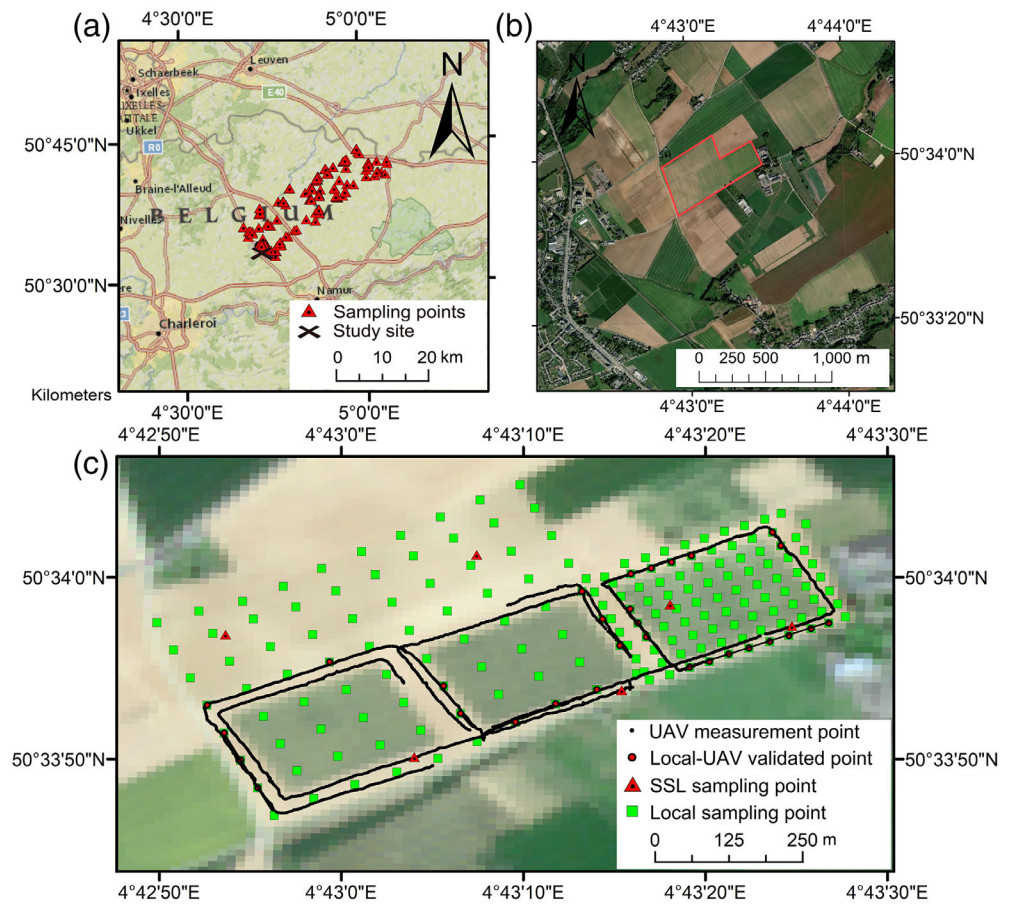
A flowchart illustrating the data and modelling approaches used in this study is shown in Figure 2. We use data from both a single field (local), where UAV-based soil spectra were acquired and which was densely sampled, and from an SSL (regional), where spectral information and SOC data are available for a region in central Belgium.

#### 2.2.1 | Local data

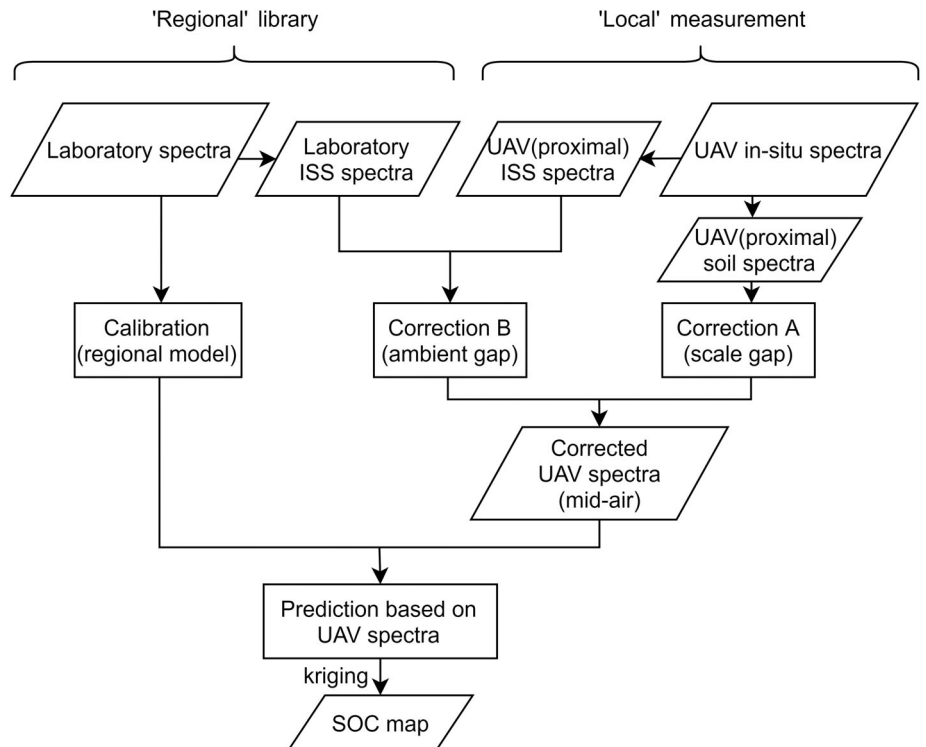
##### *UAV-based spectra*

An UAV survey was conducted in a cropland field within the aforementioned region in May 2019. The field is located ca. 1 km east of Gembloux (50.5649 N, 4.7204 E; area ca. 11 ha) and is a conventionally cultivated farmland with a winter wheat, winter barley, and sugar beet crop rotation. The fields are annually ploughed to a depth of ca. 25 cm resulting in a uniform SOC content in the plough layer (Dvorakova et al., 2020). The topography is characterized by a slightly undulated terrain with an altitude range between 161 and 168 m a.s.l. The last tillage operation was a seedbed preparation, and this resulted in a smooth and homogeneous soil surface (i.e., low roughness), which was dry with very few residues present at the soil surface (Figure 3d).

**FIGURE 1** Study site and sampling scheme of ‘regional’ SSL and ‘local’ field (a) ‘regional’ SSL: Spatial distribution of the sampling points in the Belgian Loam Belt (b) Satellite orthoimage of UAV survey region provided by Google Maps (c) ‘local’ field: Ground sampling and UAV survey on the study site. The imagery is taken from SENTINEL-2A product on one day before UAV survey [Colour figure can be viewed at [wileyonlinelibrary.com](http://wileyonlinelibrary.com)]



**FIGURE 2** Flowchart of the methodology showing the data collection and modelling approaches



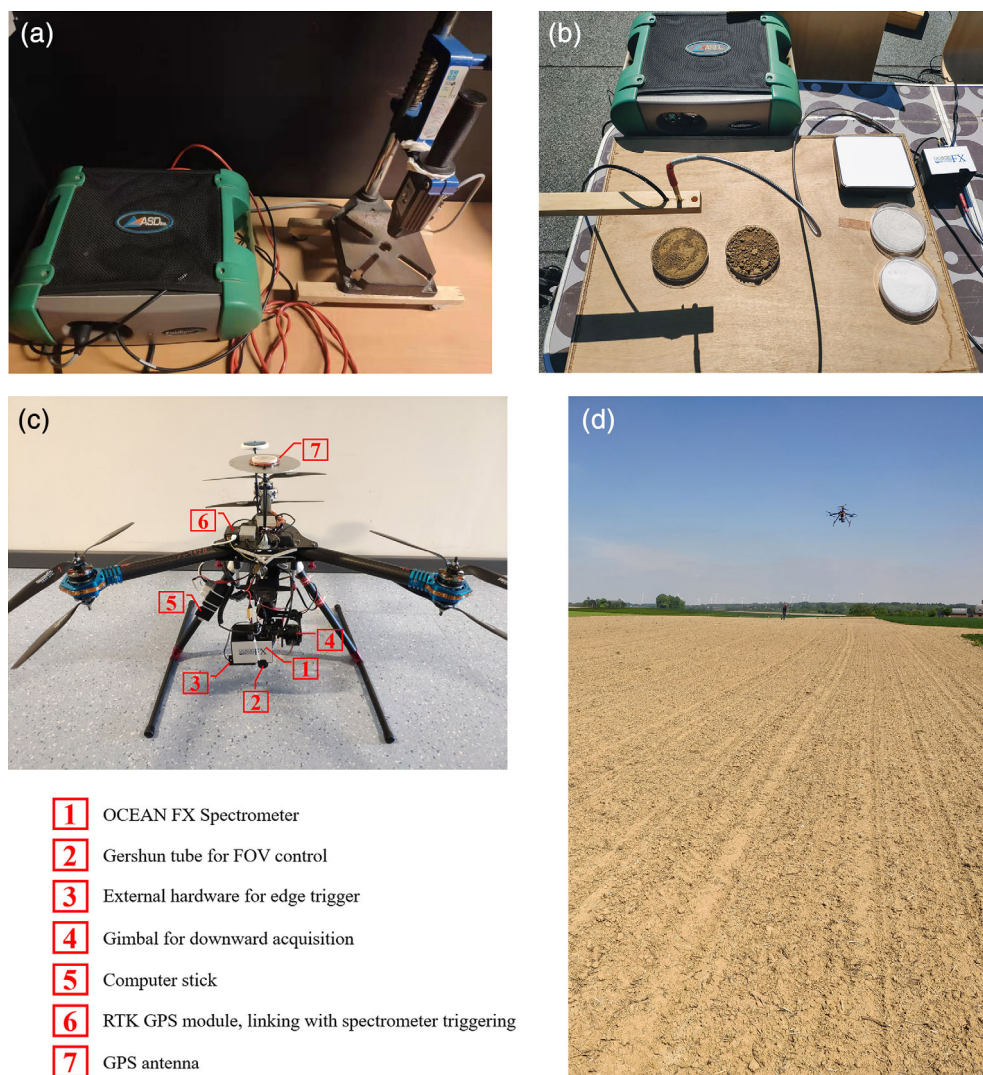


**FIGURE 3** Illustration of the three spectroscopic measurement scenarios (a) ‘laboratory’ setup: a contact-probe assembly armed with a halogen lamp (b) ‘proximal’ setup: fore optics were fixed 10 cm above the soil samples under sunlight (c,d) ‘UAV’ setup: information of main assembly parts and a demonstration of the in-situ UAV-based spectral measurement [Colour figure can be viewed at [wileyonlinelibrary.com](http://wileyonlinelibrary.com)]

The UAV-based spectral data were acquired using a portable spectrometer (OCEAN FX Spectrometer, Ocean Optics, Inc., USA) with a wavelength range between 350 and 1000 nm and a spectral resolution of ca. 0.39 nm. The FX was mounted on a high-payload aerial system (Figure 3c). This UAV platform is a custom-built hexacopter and is equipped with a DJI A2 flight controller. The total weight of the platform (spectrometer + battery + drone frame) is 5.0 kg, and the UAV has a flight time of ca. 15 min. An RTK/PPK (real-time kinematic and postprocessing kinematic) enabled multi-GNSS (global navigation satellite system) receiver was connected to the FX to synchronize the spectral acquisition with GNSS logging signals via a voltage pulse to provide a high-precision geolocation. The high-precision PPK-GNSS and the high acquisition speed (up to 4500 scans per second) of the FX spectrometer enable a centimeter-level georeferencing accuracy (Zhang et al., 2019). The spectrometer was mounted on a gimbal to ensure a vertically downward acquisition angle during the flight. The survey was conducted around 13:00 pm (i.e., solar noon) on 14 May 2019 under a cloudless sky. The FOV of the spectrometer was fixed at 8° using a Gershun fore optic tube. The flight height was ca. 15 m above the take-off point, leading to a footprint with a radius of

ca. 1.05 m on the soil surface. Three consecutive flights were performed during the data acquisition. Before each flight, the radiometric calibration was conducted using a spectralon panel. A standard soil sample (WB) was measured at a height of 10 cm as a benchmark after each radiometric calibration and before the UAV take-off (see Section 2.4.2). The acquisition interval was 1 s, and in total, 2448 valid soil spectra were acquired (Figure 1c).

#### Soil data

A set of 179 soil surface samples (0–25 cm) from this field was collected by the Walloon Agricultural Research Center (CRA-W) in August 2018 according to a regular grid (Figure 1c). We refer to this soil data set as ‘Local’ (Table 1). Sample positions were recorded using a John Deere Starfire 3000 real time kinematic (RTK) GPS instrument with 2.5 cm precision. The SOC content was analyzed by means of the dry combustion method as detailed in Dvorakova et al. (2020). This data set was related to the UAV-based spectral data under the assumption that SOC changes between the sampling and UAV flight (ca. 9 months) were not significant/measurable. Given the very slow rate of change in SOC content reported for this region, for example,

**TABLE 1** Descriptive statistics of the soil organic content and number of samples for the 'Regional', 'Local' and 'Local-UAV' datasets

Soil dataset	Description	N° samples	SOC content (g kg <sup>-1</sup> )			
			Min	Max	Mean	Sd
'Regional'	Samples from Belgian Loam Belt	128	6.67	24.72	12.55	3.71
'Local'	Samples from local study field	179	8.24	15.02	10.25	1.22
'Local-UAV'	Overlap between 'Local' and UAV-spectral data points	45	8.76	13.10	10.39	1.19

Goidts and van Wesemael (2007), we argue that is a very reasonable assumption. Forty-five of the UAV-based spectral measurements described above overlapped with sampling positions of the local soil data set (i.e., were within a horizontal distance of less than 3 m). This subset of the 'Local' soil data set is referred to as the 'Local-UAV' soil dataset in the remainder of this paper (see sample collection, Figure 1c).

### 2.2.2 | Regional data

A regional soil data set and SSL were constructed using the soil samples collected in the framework of the study of Shi et al. (2020). A total of 83 samples were randomly collected on arable fields within the larger study area in October 2018. For this study, we expanded this soil archive with 45 additional samples from bare croplands in the study area (Figure 1a). This data set is referred to as the 'Regional' soil data set in the remainder of this paper. Using a consistent sampling methodology, the 128 samples were taken from the upper 10 cm of soil. The samples were analyzed for SOC content using an elemental analyzer (see Shi et al., 2020 for a detailed description of the methodology). Although the sampling depth of the Regional soil data set (i.e., 10 cm) is different than that of the 'Local' data set (i.e., 25 cm), we argue that the difference in sampling depth between the two data sets does not induce a bias, as the study site is ploughed regularly to a depth of ca. 25 cm creating a uniform SOC content in the plough layer (Meersmans et al., 2009).

Soil spectra for this regional soil data set were measured under both laboratory and outdoor (proximal) conditions, where outdoor measurements were performed as an intermediate step to evaluate the effects of incident irradiance on in situ measurement. For the laboratory setup, Vis-NIR reflectance spectra of 2-mm sieved soil samples were obtained using an ASD FieldSpec 3 FR spectrometer (Analytical Spectral Devices Inc., USA, wavelength range: 350–2500 nm, spectral resolution: 1 nm). The measurements were conducted in a dark room, using an ASD contact probe, equipped with a built-in light source (100 W halogen reflectorized lamp, Figure 3a). The spectrometer was started 30 min prior to measurements to warm up. The outdoor proximal measurements were performed under sunlight with a cloudless sky using a portable FX spectrometer (which was also used in the UAV surveys). To simulate the in situ soil surface conditions, bulk soil samples without presieving were measured by the FX spectrometer fitted with a fore optic accessory (Gershun tube) with field of view (FOV) of 8°. The distance between the fore optic

and the soil samples was fixed at 10 cm. This setup was chosen to simulate the UAV in situ scenario where reference scans were performed before taking off. Soil samples were placed in Petri dishes, and the spectral acquisition was conducted from 12:00 am to 2:00 pm (within 2 h of local noon).

### 2.3 | Pretreatment of spectral data

Given that the two spectrometers (i.e., ASD and FX) have different spectral ranges and resolutions, we resampled the ASD spectra to fit the FX bands. Noisy segments at wavelengths below 400 nm and beyond 900 nm were removed, retaining 400–900 nm range with resolution of ca. 0.39 nm. To smooth the signal, the Savitzky-Golay filter was applied (Savitzky & Golay, 1964) with a third-order polynomial fit and a window size of 59 data points due to the high spectral resolution. Derivative processing was not applied because the NIR reflectance of the proximal measurement was sensitive to the changed footprint (see Figure 5a).

### 2.4 | SOC predictive models

The processed spectral matrix was related to measured SOC values with multivariate regression algorithms. Partial least square regression (PLSR) was used to build spectral transfer functions for the prediction of SOC. To avoid over- or underfitting, the optimal number of variables was determined as the one producing a model having the minimal root mean square error (RMSE) of cross-validation. Two calibration approaches were evaluated: (i) one based on the local soil dataset (local model) and (ii) one based on the regional SSL (regional model).

#### 2.4.1 | Local model

The local model was constructed using the 'Local-UAV' soil data set and the UAV-based spectra ( $n = 45$ ). The calibration data set was selected as a subset of the 'Local-UAV' data set using the Kennard-Stone (KS) algorithm, which selects a subset with a uniform distribution over the predictor space so as to increase the diversity of the calibration set (Kennard & Stone, 1969). We used two-thirds ( $n = 30$ ) of the observations to calibrate the predictive model, while the remainder ( $n = 15$ ) for validation. Capitalizing on the high spectral resolution,

the models can be optimized by using a band-selection approach, which assembles partial least-squares regression (PLSR), random forest (RF), and support vector machine (SVM) to designate the most important spectral bands to improve SOC prediction, as detailed in Feilhauer et al. (2015) and Laamrani et al. (2019). After this selection procedure, PLSR models were calibrated using only the selected bands. We report the SOC prediction performance in Figure 4 and the detailed band selection in Appendix (Figure A1). The model performance metrics used include root mean square error [RMSE; Equation (1)], coefficient of determination ( $R^2$ ), ratio of the performance to deviation [RPD; Equation (2)], and ratio of performance to interquartile range [RPIQ; Equation (3)].

$$RMSE = \sqrt{\frac{\sum_{i=1}^n (y_o - y_p)^2}{n}} \quad (1)$$

$$RPD = \frac{\sigma}{RMSE} \quad (2)$$

$$RPIQ = \frac{IQ}{RMSE} \quad (3)$$

Where:  $y_o$  is the observed and  $y_p$  is the predicted value,  $n$  is the number of the samples,  $\sigma$  is the standard deviation, and IQ is the interquartile range. The threshold values of RPD defined by Chang et al. (2001) are widely used in soil spectroscopy literature to assess the model accuracy:

excellent prediction capability when  $RPD > 2$ , intermediate capability when  $1.4 < RPD < 2$  and to be unreliable when  $RPD < 1.4$ . The RPIQ values were also reported to consider the range of variation for data with a nonnormal distribution as suggested by Bellon-Maurel et al. (2010).

## 2.4.2 | Regional model

The regional model was constructed using the laboratory spectral measurements and SOC data from the 'Regional' soil data set (Regional SSL). Given that the soil spectra of the regional SSL and UAV-based spectra were measured under different conditions (see Table 2), a spectral alignment procedure was applied to eliminate the discrepancy of spectral readings. According to Kopačková & Ben-Dor (2016), the spectral measurements under diverse measurement conditions or instrumentation factors can be aligned by using an ISS to deal with systematic bias. The soil standard was measured in each setup as the 'standard spectrum' for correcting the slave setup (i.e., UAV-based) to the benchmark setup (i.e., Regional SSL) [Equations (4) and (5)]:

$$C_\lambda = 1 - ((\rho_{s,\lambda} - \rho_{BM,\lambda}) / \rho_{s,\lambda}) \quad (4)$$

$$R_{c,\lambda} = R_{o,\lambda} \times C_\lambda \quad (5)$$

Where:  $\lambda$  is a given wavelength,  $\rho_{s,\lambda}$  is the reflectance of the ISS measured at the slave setup,  $\rho_{BM,\lambda}$  is the reflectance of the ISS measured

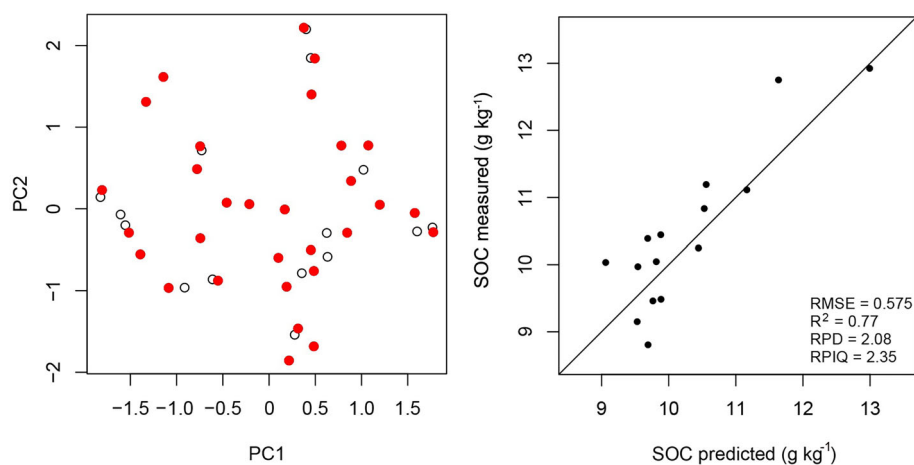


**FIGURE 4** SOC prediction using the local model. The left panels show the selection of calibration samples (red) using the Kennard-Stone algorithm. Projections of the spectra into the principal component space defined by the first two principal components in each calibration. The right panels show the measured versus predicted SOC. The RMSE is given as  $\text{g C kg}^{-1}$  [Colour figure can be viewed at [wileyonlinelibrary.com](http://wileyonlinelibrary.com)]

**TABLE 2** Comparison of spectral measurement conditions

	Regional SSL		Local data
	Laboratory	Proximal	UAV-based
Sensor	ASD	FX	FX
Spectral range	350–2500 nm	350–1000 nm	350–1000 nm
Incident light	Halogen lamp	Sunlight	Sunlight
Sensor to soil distance	Contact	10 cm	15 m
Soil condition	Sieved soil	Bulk soil	Seedbed
Perturbing factors	None	Incident irradiance, roughness	Incident irradiance, roughness, footprint of sensor, and so on.

at laboratory setup,  $R_{o,\lambda}$  is the original soil sample reflectance (the soil spectrum measured at the slave setup),  $R_{c,\lambda}$  is the corrected soil sample reflectance (the soil spectrum measured at the slave setup normalized to the benchmark setup), and  $C_\lambda$  is a correction factor.

To evaluate the suitability of this transfer procedure, we first assessed the alignment between ‘proximal’ and ‘laboratory’ spectra for the ‘Regional’ soil data. We used one single soil sample from the Regional data as the standard to perform the alignment between laboratory and proximal spectral measurements. Then the SOC contents were predicted by applying laboratory-SSL-based prediction model on the aligned proximal spectra. To evaluate the robustness of this approach, we repeated this procedure 128 times by changing the standard sample selected from the Regional soil dataset. The prediction performance was estimated by cross-validation where we used 70% of the data as a training set and 30% as a validation set, with 128 repetitions.

The UAV spectral measurement were aligned to the proximal spectral measurements of the regional SSL. The alignment procedure was implemented as follows: First, a scan of an ISS [WB standard sand, detailed in Ben Dor et al. (2015)] before each UAV take-off was used to eliminate the potential bias during white calibration caused by the different FOV of the sensor during flight. In addition, we took a single soil sample which was collected beneath the UAV survey path on the study field. This sample was scanned during the flight as well as in the proximal measurement setup (i.e., at 10 cm above the samples, see above). As a result, the alignment process was performed in two steps based on: (i) a proximal observation and a UAV-based observation at the same location. Given the homogeneity of the seed-bed condition of soil surface, we consider the difference in spectral readings between the proximal and UAV-based measurements as systematic. This discrepancy is related to the distance between the sensor and the soil surface and is defined as the *scale effect* (ii) on a proximal and UAV-based measurement of an ISS (WB standard sand). Given the different illumination conditions, we consider that the difference is related to the light conditions and refer to this as the *ambient effect*. The overall correction factor that allows to transfer the spectra can then be obtained by combining the scale and ambient effects. Finally, a subset of SSL using the KS algorithm was determined ( $n = 38$ , with minimum RMSE of calibration) for calibrating the regional model, and the 45 aligned ‘Local-UAV’ spectra were assigned as external validation to assess the prediction accuracy.

## 2.5 | SOC prediction and mapping

For SOC mapping, the SOC contents of the UAV-based observation points ( $n = 2448$ ) were predicted using the local and regional prediction models described above. Spatially continuous SOC maps were created using Empirical Bayesian kriging in ArcMap 10.4 (ESRI) and the point SOC predictions. The inner part of the field was masked out due to crop cover (Figure 1). Two SOC maps were derived: (i) based on the local model (SOC map A) and (ii) based on the regional model (SOC map B). In addition, given the very high sampling density of the

‘Local’ soil data set (i.e., 179 samples), a SOC map was created using kriging interpolation as a reference (SOC map C). Using this reference map, prediction error maps were generated. To visualize the detailed variation of the SOC maps, three representative transects along the elevation gradient were extracted from each SOC map for comparison.

## 3 | RESULTS

### 3.1 | Summary of soil properties

The SOC content of ‘Regional’ soil dataset varied from 6.67 to 24.72 g kg<sup>-1</sup> with a mean value of 12.55 g kg<sup>-1</sup> and a standard deviation (Sd) of 3.71 g kg<sup>-1</sup> for the 128 samples (Table 1). The ‘local’ soil dataset contained 179 samples with SOC values ranging between 8.24 and 15.02 g kg<sup>-1</sup> (Sd of 1.22 g kg<sup>-1</sup>). The ‘Local-UAV’ soil dataset contained 45 samples with a smaller range (8.76–13.10 g kg<sup>-1</sup>) and Sd (1.19 g kg<sup>-1</sup>).

### 3.2 | Local model

The local model shows good performance in SOC prediction using UAV-based spectra (Figure 4). The RMSE is 0.57 g kg<sup>-1</sup>, with an RPD of 2.08 and an RPIQ of 2.35. The band-selection results are shown in Figure A1, and the ensemble approach improved the predictive accuracy of the local model.

### 3.3 | Regional model with spectral alignment

The laboratory and proximal measurements result in spectral curves with similar shape and magnitude (Figure 5). The proximal spectra acquired with the fore optic (i.e., smaller FOV) shows random noise at wavelengths beyond 800 nm and the reflectance was lower compared to those obtained by laboratory measurements. The UAV measurements (in-situ, at the height of ca. 15 m) result in a distinctly different reflectance curve from 550 nm onwards. In order to understand this signal, we first report on the alignment between proximal and laboratory spectra (Figure 5b). A correction factor emerged, ranging between 0 and 1.3, showing that the proximal measurement slightly underestimated the reflectance relative to laboratory measurements. In a second step, we relate the UAV- and proximal spectra. The procedure to align the UAV-based spectra to laboratory spectra is shown in Figure 5(c)–(f). The correction factor for scale effect ranged from 0.8 to 1.2 and the correction factor for ambient effect ranged from ca. 1 to 1.15. When multiplying the two ratios, the correction coefficient showed a steady growing trend from 0.8 to 1.4 with increasing wavelength. The aligned reflectance curve of the UAV measurement showed similar magnitude and slope as the laboratory measurement. Figure 6 shows the prediction results of the SSL-based regional models applied on the aligned proximal spectra. The use of a single

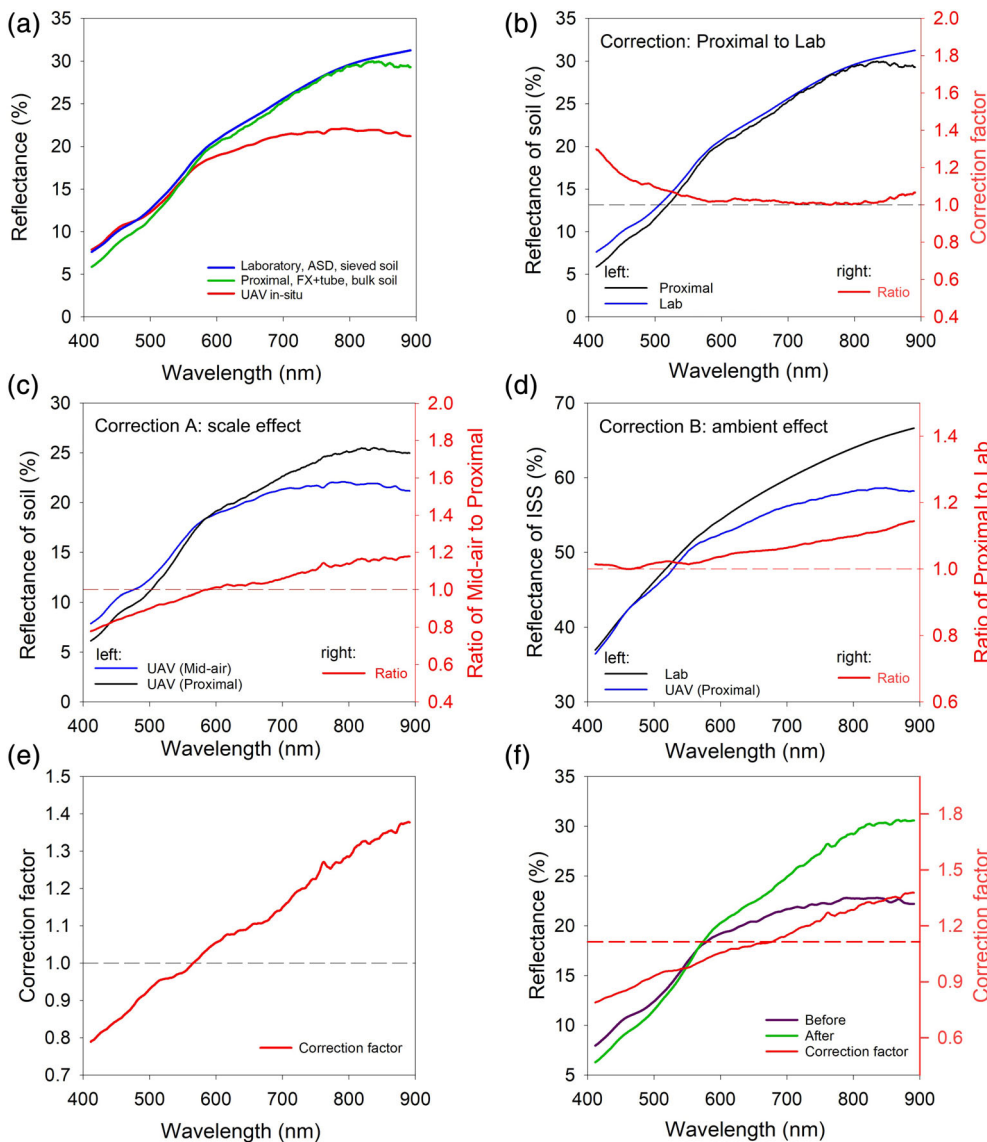


**FIGURE 5** (a) One soil sample measured from different setups illustrating the discrepancy in spectral readings. (b) The spectral alignment between proximal and laboratory measurement. (c) Correction for scale effect based on soil spectrum measured from Mid-air and from proximal, respectively (d) Correction for ambient effect based on ISS spectral measurement at laboratory and proximal conditions, respectively (e) Correction factor calculated from multiplying ratio A and ratio B (f) Applying the correction coefficient to transfer the UAV (Mid-air) spectral data into the laboratory condition [Colour figure can be viewed at [wileyonlinelibrary.com](http://wileyonlinelibrary.com)]

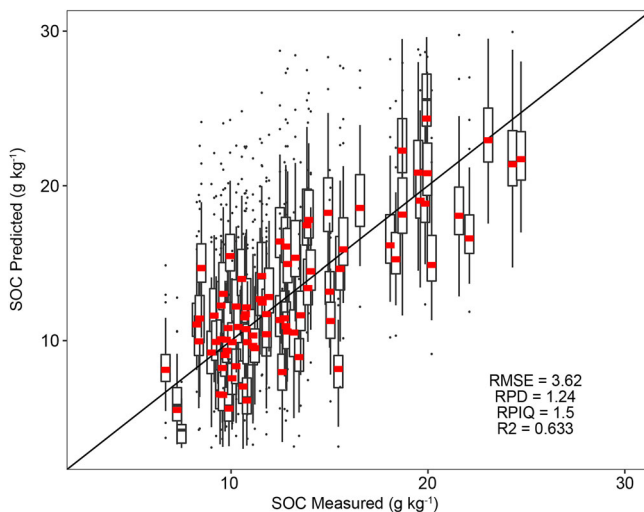


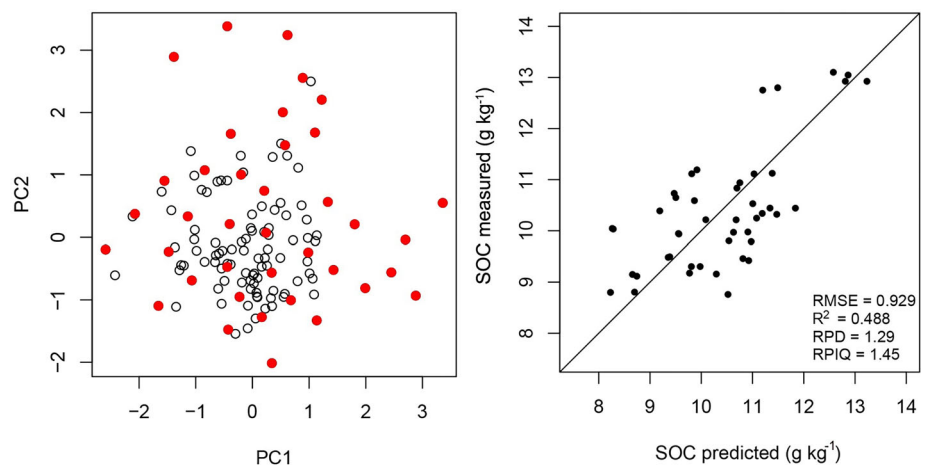
**FIGURE 6** SOC prediction using laboratory-based regional model on aligned proximal spectra. The boxplot indicates the predicted values of each observation in the repeated cross-validation [Colour figure can be viewed at [wileyonlinelibrary.com](http://wileyonlinelibrary.com)]

soil sample as standard shows a strong capability to perform the alignment: the SOC predictions were mostly accurate ( $R^2 = 0.63$ ,  $RPIQ = 1.5$ ), also when using different soil samples to align the measurements. This suggests that the SSL-based (laboratory) model is transferable to the aligned proximal spectra. Similarly, the UAV-based aligned spectra, comparing to original spectra, had improved prediction in combination with the regional model (Table A1). It provides a lower, but still fair prediction capability for SOC with an  $R^2$  of 0.49 and an  $RPIQ$  of 1.45 (Figure 7).

### 3.4 | SOC mapping

SOC maps generated using the three approaches are shown in Figure 8. The UAV-based SOC maps show more spatial details relative to the ground sampling-based estimation (SOC map C) due to the higher spatial sampling resolution (Figure 8b). Although differences in the spatial patterns among the three maps are notable, they consistently show higher SOC contents mainly on the toeslope (south of the

**FIGURE 7** SOC prediction using the regional model. The left panels show the selection of calibration samples (red) using the Kennard-Stone algorithm. Projections of the spectra into the principal component space defined by the first two principal components in each calibration. The right panels show the measured versus predicted SOC. The RMSE is given as  $\text{g C kg}^{-1}$  [Colour figure can be viewed at [wileyonlinelibrary.com](http://wileyonlinelibrary.com)]



field, Figure 8b). The prediction based on the UAV-based spectra and the local model shows a similar SOC range and mean value ( $10.68$  and  $10.61 \text{ g kg}^{-1}$ ) as the reference map (i.e. map C based on ground sampling). In contrast, the map derived from the regional model shows a slight bias of  $\text{ca.}0.8 \text{ g kg}^{-1}$ , which is consistent with the RMSE of the SSL-based predictive model ( $0.93 \text{ g kg}^{-1}$ ). The error maps of local and regional models show a similar spatial distribution of the prediction error, while the (regional) map shows a higher bias and an underestimation of the SOC contents (Figure 8c). The SOC values extracted from the three transects show the same trend as observed with the reference map (map C) Figure 8d). A slight bias can be observed between UAV (local)- and UAV (regional)-derived predictions, the magnitude of which was in accordance with the bias observed from the density plot.

## 4 | DISCUSSION

### 4.1 | Capability of UAV-borne spectrometry for SOC mapping

Our results demonstrated that UAV-based hyperspectral measurements can be an effective method for assessing the surface SOC content of bare cropland. Both local- and SSL-based calibrations provided acceptable predictions of within-field SOC patterns at very high spatial resolution. As expected, the use of in-situ data to construct a local model resulted in a high prediction accuracy ( $\text{RMSE} = 0.58 \text{ g kg}^{-1}$ ,  $\text{RPIQ} = 2.35$ ). However, this accuracy comes at a high cost as it requires detailed local soil sampling and chemical analysis. In contrast, the regional model utilizes an existing SSL, which can substantially decrease the need for in-situ sampling, thereby providing a more time- and cost-effective workflow. However, the prediction based on the regional SSL-model had less accuracy ( $\text{RMSE} = 0.93 \text{ g kg}^{-1}$ ,  $\text{RPIQ} = 1.45$ ) and had a bias. The errors associated with the regional SSL-based prediction is probably related to two aspects: first, during the alignment of the UAV-based spectra with laboratory measurements that were used to populate the SSL, the application of a

transfer function inevitably induces noise and bias. Second, using regional calibrations to make predictions at local scales are usually challenging when the local dataset has smaller range of variation (Guerrero et al., 2014; Stenberg et al., 2010). However, the prediction is still a good representation in terms of the relative variation of SOC values at the field scale, which provides useful information for field-scale management or for designing an optimal sampling strategy in the context of SOC monitoring. Likewise, this method can provide a precise estimation of the variances within the strata, which can assist the sample size determination in strata by Neyman allocation (de Gruijter et al., 2015). In addition, the spatialized spectral data as ancillary information can also be used for downscaling existing SOC maps (e.g., Malone et al., 2017).

It should be noted that the SOC variation in this study was relatively small compared to other studies using UAV-based spectroscopy (Aldana-Jague et al., 2016; Biney et al., 2021; Laamrani et al., 2019). The successful prediction of SOC using UAV-derived spectra demonstrates an adequate performance and sensitivity of hyperspectral sensor to derive effective information from noisy signals (caused by surface disturbing conditions) given the fine spectral resolution, even when the variation range of the target variable is small. This is important for UAV-based field-scale monitoring as soil properties within a single field tend to have limited variability.

### 4.2 | Potential of high spectral resolution for model optimization

Several studies have investigated using multispectral (Aldana-Jague et al., 2016; Biney et al., 2021) and hyperspectral (Laamrani et al., 2019) imaging sensors on UAV platforms to assess SOC contents. As opposed to imaging sensors, the point spectrometer used in this study provides very high spectral resolution at less than  $1 \text{ nm}$ , but has a limited capability to identify ground objects. The use of point spectrometers therefore requires the precise geotagging during the data acquisition. Here, we integrated the PPK (post-processing kinematic) positioning technique with the triggering system of the

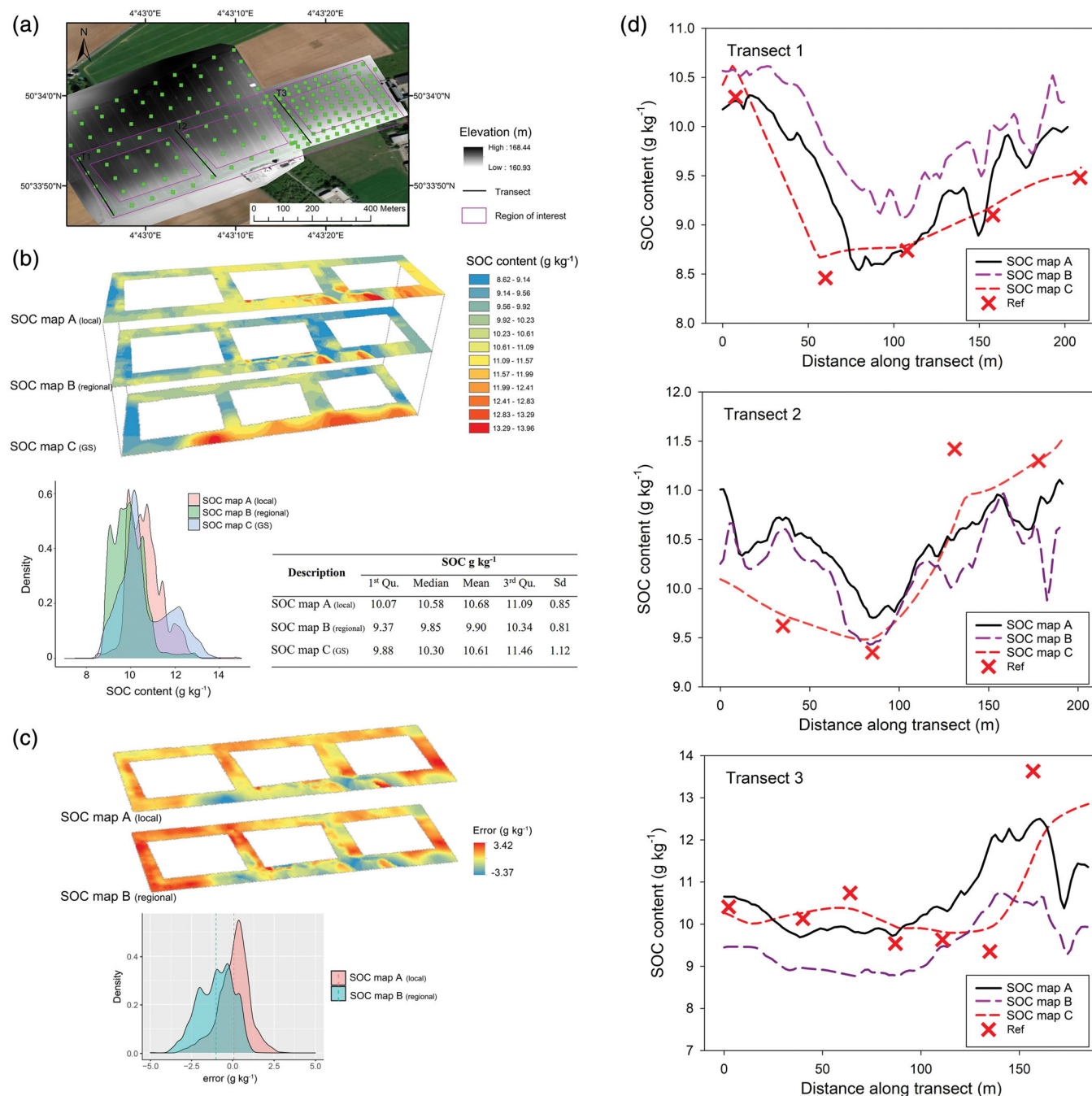


**FIGURE 8** Comparison of the kriging SOC maps. (a) Location of the transects and the region of interest in the study field with a topographic overview. Region of interest shows the overlap region both UAV survey and ground survey covered (b) Spatial SOC prediction on region of interest by the three approaches. UAV (local): Prediction model calibrated using the in-situ local data; UAV (regional): Prediction model calibrated using the library-based regional data; GS: Ground sampling-based kriging map (c) Error maps of the region of interest. The density plot shows the distribution of error using GS map as reference (d) The three extracted transects showing SOC values derived from the three maps. Ref: Measured value regarded as reference points [Colour figure can be viewed at [wileyonlinelibrary.com](http://wileyonlinelibrary.com)]

spectrometer, enabling a centimetre-level accuracy during spectral acquisition. In addition, the fine spectral resolution enables the band-selection by the ensemble modelling approach (Du et al., 2012; Feilhauer et al., 2015; Laamrani et al., 2019). With the specific bands or regions sensitive to SOC content being selected and the bands of low SNR (Signal-to-noise Ratio) removed, the prediction performance

was improved. When the band-selection approach applied on different measurement setups (Figure A1), the results showed different effects: For the laboratory and proximal measurements, the important bands were found in 410–440, 540–570 and 880–900 nm, which were in accordance with other studies using single modeling approach (i.e., PLSR) for selecting important bands when predicting carbon. For

example, Sarkhot et al. (2011) identified wavelengths 358, 378–438, 498–768, 728–1148 nm in the Vis–NIR region as important for the estimation of total carbon in the soil. For UAV measurements, the important bands (i.e., around ca. 500 nm and 880 nm) were consistent with those obtained under laboratory or proximal conditions. This suggests that the position of diagnostic bands is related to the mineral composition of the soil itself (Nocita et al., 2015), and does not vary with measurement conditions or factors such as texture (i.e., particle size fraction) or moisture (Laamrani et al., 2019). In our case, the local model based on UAV spectra benefited most from the band-selection where the RPIQ increased from 1.5 to 1.9, while it was less effective on the laboratory and proximal conditions where a slight amelioration was observed in UAV measurement. These results indicate that the band-selection approach is more effective when data contains more random noise.

### 4.3 | Spectral transfer procedure

Based on our assessment of the spectral alignment procedures, we showed that differences in reflectance readings exist but that these can be regarded as a systematic bias and the robustness of the SOC prediction models is still good. UAV-based spectral measurement can be considered as another form of ‘proximal’ measurement but with more perturbing factors that need to be considered, including: (i) disturbance of field surface characteristics such as soil roughness and moisture content (Croft et al., 2012; Wu et al., 2009); (ii) temporal variations in anisotropic hemispherical illumination characteristics, solar zenith angle changes, atmospheric scattering (Anderson et al., 2011); (iii) field-of-view (FOV) of the fore optic and the spatially related responsivity of field spectrometers (MacArther et al., 2013); (iv) the distance between the sensors and objects (Kamal et al., 2017; Kipp et al., 2014). These factors, together with BRDF effects, complicate spectral measurements and further research is needed to isolate these effects. Nevertheless, as demonstrated in the alignment between laboratory measurement of sieved soil and proximal measurement of bulk soil, the spectral features were robust either under controlled (halogen lamp) or solar illumination. Based on this, we showed the discrepancy of spectral readings between different measurement conditions as systematic bias and therefore, the SOC prediction models are transferable after proper alignment. Given the optimal soil condition (dry seedbed without residue) and weather condition (clear sky), we simplified these factors into two main aspects, that is, a footprint-induced scale effect and an ambient condition-induced effect. Consequently, the alignment procedure using the ISS concept (Kopačková & Ben-Dor, 2016) was applied in two steps: First, the ambient effect involved illumination conditions and irradiance measurement. The illumination under laboratory conditions was stable and strictly defined by the light intensity and angle, while it may be varying during in-situ measurements. Also, when measuring irradiance in the field, a coarse control of the measurement geometry between Lambertian reference panel and the incident light could lead to a bias. Our study showed that the spectral alignment using an ISS provides a robust mean to address these issues. Regarding the scale effect, it is

probably a combined effect of reflectance anisotropy of the soil surface, measurement geometry and footprint (e.g., Aasen et al., 2018). Theoretically, a direct radiometric correction using a spectralon panel (measuring the down-welling irradiance) at mid-air would be the ideal solution but it requires a large reference panel and accurate positioning of the UAV, which is not practical. In our approach, we aligned one proximal and one mid-air observation from the same location (which can be acquired during the UAV takeoff phase), under the condition that the soil is homogenous in terms of roughness and moisture. Therefore, we suggest that such a correction should be conducted per field (i.e., under the same surface condition). In a pre-experiment, we measured the spectral reflectance over a ploughed field with random positions within 1 m<sup>2</sup> at different height and investigated the standard deviation of the spectra of the repeated measurements at variable heights (Figure A2). The result showed that the observations at higher altitude had lower standard deviation than those of lower altitudes. This indicates the larger footprint has averaged the shadow-caused signal deviations and the spectral features become more homogeneous. From a height of ca. 2 m, we obtained relatively stable spectra which supports the assumption for the ‘scale’ correction applied in this study. The two-step correction procedure as well as the SSL-based SOC mapping workflow is summarized in Figure A3. However, since the study was conducted in a homogenous field, the effect of disturbing factors such as soil roughness, moisture and residues cover were not investigated. Further work is required to test the replicability of the results by performing the UAV flight under varying sunlight and surface conditions, and to seek correction methods to address the noise and bias that might be caused by those disturbances.

### 4.4 | Limitations and outlook

With the spectral alignment paving the way of exploiting SSL-based model on UAV-based spectra, the key challenge for improving accuracy turns into how to effectively use global/regional calibrations to predict local variation in SOC content. In this study, the use of the Kennard-Stone algorithm to select a subset for calibration has improved the model performance to some extent, yet efforts are still needed on predicting narrow variation of SOC content from a general model. Overall, this study proposed a first basic workflow to integrate field-scale UAV-based approaches with SSLs. We demonstrated that there is a potential to reduce the need for sampling and analytical efforts by using SSL-based models. Along with the generalization of open-access SSLs, this technique can have a wide range of applications for measuring/monitoring soil properties efficiently.

## 5 | CONCLUSIONS

This study presented and evaluated a methodology to derive SOC estimations for bare cropland soils using a UAV-borne spectrometer. Two calibration approaches (based on local sampling and regional SSL,

respectively) were evaluated and both showed good capability for SOC content prediction. For the local calibration, the prediction can be optimized by band-selection approach to obtain an improved prediction performance (RPIQ = 2.35, RMSE = 0.57 g kg<sup>-1</sup>). For the regional model, due to the discrepancy in spectral measurements, a spectral alignment procedure needs to be applied so that the SSL-based regional model can be applied to UAV-based spectra for SOC prediction. Finally, we demonstrated that the use of an SSL-based regional model had a fair predictive capability for local SOC prediction, albeit with a lower performance than approaches relying on local sampling (RPIQ = 1.45, RMSE = 0.93 g kg<sup>-1</sup>). This has the potential to reduce the need for high resolution in-situ sampling, thereby providing a more time- and cost-efficient workflow. The comparison of SOC maps derived from the three approaches (i.e., SSL-based regional model, in-situ-based local model and sampling-based interpolation) showed high consistency, suggesting that UAV-based spectral measurements, in combination with SSLs has the potential to improve the efficiency in SOC mapping and precision agriculture.

## ACKNOWLEDGMENTS

This research was funded by the Belgian Federal Science Policy Office (BELSPO) as part of the UAVSOIL project 'UAV borne spectrometers for high resolution soil and crop monitoring' (Contract SR/00/362) and by the China Scholarship Council (Grant No. 201706300034).

## CONFLICT OF INTEREST

The authors declare no conflicts of interest.

## DATA AVAILABILITY STATEMENT

Data available on request from the authors

## ORCID

He Zhang  <https://orcid.org/0000-0003-0328-1445>

## REFERENCES

- Aasen, H., Honkavaara, E., Lucieer, A., & Zarco-Tejada, P. J. (2018). Quantitative remote sensing at ultra-high resolution with UAV spectroscopy: A review of sensor technology, measurement procedures, and data correction workflows. *Remote Sensing*, *10*(7), 1091. <https://doi.org/10.3390/rs10071091>
- Aldana-Jague, E., Heckrath, G., Macdonald, A., van Wesemael, B., & Van Oost, K. (2016). UAS-based soil carbon mapping using VIS-NIR (480-1000 nm) multi-spectral imaging: Potential and limitations. *Geoderma*, *275*, 55–66. <https://doi.org/10.1016/j.geoderma.2016.04.012>
- Anderson, K., Dungan, J. L., & MacArthur, A. (2011). On the reproducibility of field-measured reflectance factors in the context of vegetation studies. *Remote Sensing of Environment*, *115*(8), 1893–1905. <https://doi.org/10.1016/j.rse.2011.03.012>
- Ballabio, C., Panagos, P., & Monatanarella, L. (2016). Mapping topsoil physical properties at European scale using the LUCAS database. *Geoderma*, *261*, 110–123. <https://doi.org/10.1016/j.geoderma.2015.07.006>
- Bellon-Maurel, V., Fernandez-Ahumada, E., Palagos, B., Roger, J. M., & McBratney, A. (2010). Critical review of chemometric indicators commonly used for assessing the quality of the prediction of soil attributes by NIR spectroscopy. *TrAC - Trends in Analytical Chemistry*, *29*(9), 1073–1081. <https://doi.org/10.1016/j.trac.2010.05.006>
- Ben Dor, E., Ong, C., & Lau, I. C. (2015). Reflectance measurements of soils in the laboratory: Standards and protocols. *Geoderma*, *245–246* (January), 112–124. <https://doi.org/10.1016/j.geoderma.2015.01.002>
- Biney, J. K. M., Saberioon, M., Borůvka, L., Houška, J., Vašát, R., Agyeman, P. C., Coblinski, J. A., & Klement, A. (2021). Exploring the suitability of uas-based multispectral images for estimating soil organic carbon: Comparison with proximal soil sensing and spaceborne imagery. *Remote Sensing*, *13*(2), 1–19. <https://doi.org/10.3390/rs13020308>
- Brown, D. J., Bricklemeyer, R. S., & Miller, P. R. (2005). Validation requirements for diffuse reflectance soil characterization models with a case study of VNIR soil C prediction in Montana. *Geoderma*, *129*(3–4), 251–267. <https://doi.org/10.1016/j.geoderma.2005.01.001>
- Castaldi, F., Chabrilat, S., Chartin, C., Genot, V., Jones, A. R., & van Wesemael, B. (2018). Estimation of soil organic carbon in arable soil in Belgium and Luxembourg with the LUCAS topsoil database. *European Journal of Soil Science*, *69*(4), 592–603. <https://doi.org/10.1111/ejss.12553>
- Castaldi, F., Chabrilat, S., Jones, A., Vreys, K., Bomans, B., & van Wesemael, B. (2018). Soil organic carbon estimation in croplands by hyperspectral remote APEX data using the LUCAS topsoil database. *Remote Sensing*, *10*(2), 153. <https://doi.org/10.3390/rs10020153>
- Chabrilat, S., Ben-Dor, E., Cierniewski, J., Gomez, C., Schmid, T., & van Wesemael, B. (2019). Imaging spectroscopy for soil mapping and monitoring. *Surveys in Geophysics*, *40*(3), 361–399. <https://doi.org/10.1007/s10712-019-09524-0>
- Chang, C.-W., Laird, D. A., Mausbach, M. J., & Hurburgh, C. R. (2001). Near-Infrared reflectance spectroscopy-principal components regression analyses of soil properties. *Soil Science Society of America Journal*, *65*(2), 480–490. <https://doi.org/10.2136/sssaj2001.652480x>
- Croft, H., Anderson, K., & Kuhn, N. J. (2012). Reflectance anisotropy for measuring soil surface roughness of multiple soil types. *Catena*, *93*, 87–96. <https://doi.org/10.1016/j.catena.2012.01.007>
- de Gruijter, J. J., McBratney, A. B., Minasny, B., Wheeler, I., Malone, B. P., & Stockmann, U. (2016). Farm-scale soil carbon auditing. *Geoderma*, *265*, 120–130. <https://doi.org/10.1016/j.geoderma.2015.11.010>
- De Gruijter, J. J., Minasny, B., & Mcbratney, A. B. (2015). Optimizing stratification and allocation for design-based estimation of spatial means using predictions with error. *Journal of Survey Statistics and Methodology*, *3*(1), 19–42. <https://doi.org/10.1093/jssam/smu024>
- Du, P., Xia, J., Chanussot, J., & He, X. (2012). Hyperspectral remote sensing image classification based on the integration of support vector machine and random forest. *International Geoscience and Remote Sensing Symposium (IGARSS)*, 174–177. <https://doi.org/10.1109/IGARSS.2012.6351609>
- Dvorakova, K., Shi, P., Limbourg, Q., & van Wesemael, B. (2020). Soil organic carbon mapping from remote sensing: The effect of crop residues. *Remote Sensing*, *12*(12), 1913. <https://doi.org/10.3390/rs12121913>
- Feilhauer, H., Asner, G. P., & Martin, R. E. (2015). Multi-method ensemble selection of spectral bands related to leaf biochemistry. *Remote Sensing of Environment*, *164*, 57–65. <https://doi.org/10.1016/j.rse.2015.03.033>
- Goetz, A. F. H., Vane, G., Solomon, J. E., & Rock, B. N. (1985). Imaging spectrometry for Earth remote sensing. *Science*, *228*(4704), 1147–1153. <https://doi.org/10.1126/science.228.4704.1147>
- Goidts, E., & van Wesemael, B. (2007). Regional assessment of soil organic carbon changes under agriculture in Southern Belgium (1955–2005). *Geoderma*, *141*(3–4), 341–354. <https://doi.org/10.1016/j.geoderma.2007.06.013>
- Guerrero, C., Stenberg, B., Wetterlind, J., Viscarra Rossel, R. A., Maestre, F. T., Mouazen, A. M., Zornoza, R., Ruiz-Sinoga, J. D., & Kuang, B. (2014). Assessment of soil organic carbon at local scale with spiked NIR calibrations: Effects of selection and extra-weighting on

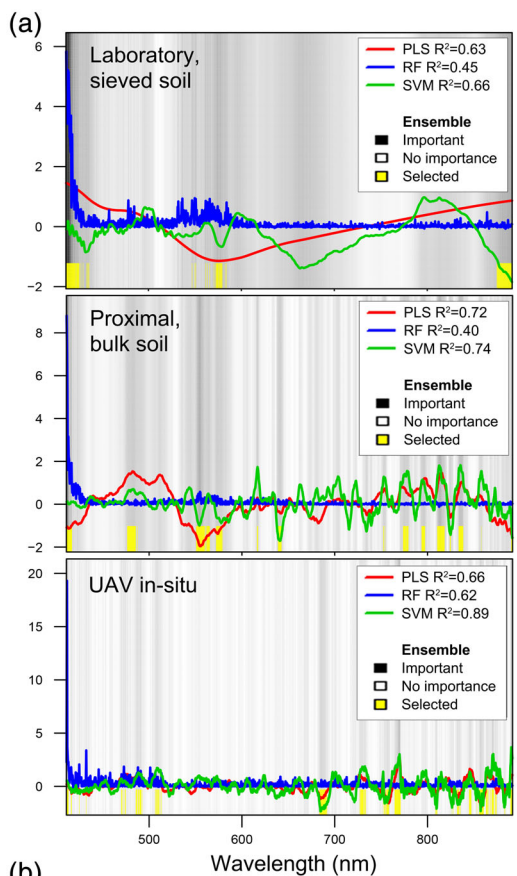
- the spiking subset. *European Journal of Soil Science*, 65(2), 248–263. <https://doi.org/10.1111/ejss.12129>
- Guerrero, C., Wetterlind, J., Stenberg, B., Mouazen, A. M., Gabarrón-Galeote, M. A., Ruiz-Sinoga, J. D., Zornoza, R., & Viscarra Rossel, R. A. (2016). Do we really need large spectral libraries for local scale SOC assessment with NIR spectroscopy? *Soil and Tillage Research*, 155, 501–509. <https://doi.org/10.1016/j.still.2015.07.008>
- Kamal, M., Ningam, M. U. L., & Alqorina, F. (2017). The effect of field spectral reflectance measurement distance to the spectral reflectance of *Rhizophora stylosa*. *IOP Conference Series: Earth and Environmental Science*, 98(1), 012059. <https://doi.org/10.1088/1755-1315/98/1/012059>
- Kennard, R. W., & Stone, L. A. (1969). Computer aided design of experiments. *Technometrics*, 11(1), 137–148. <https://doi.org/10.1080/00401706.1969.10490666>
- Kipp, S., Mistle, B., & Schmidhalter, U. (2014). The performance of active spectral reflectance sensors as influenced by measuring distance, device temperature and light intensity. *Computers and Electronics in Agriculture*, 100, 24–33. <https://doi.org/10.1016/j.compag.2013.10.007>
- Kopačková, V., & Ben-Dor, E. (2016). Normalizing reflectance from different spectrometers and protocols with an internal soil standard. *International Journal of Remote Sensing*, 37(6), 1276–1290. <https://doi.org/10.1080/01431161.2016.1148291>
- Laamrani, A., Berg, A. A., Voroney, P., Feilhauer, H., Blackburn, L., March, M., Dao, P. D., He, Y., Martin, R. C. (2019). Ensemble Identification of Spectral Bands Related to Soil Organic Carbon Levels over an Agricultural Field in Southern Ontario, Canada. *Remote Sensing*, 11(11), 1298. <https://doi.org/10.3390/rs11111298>
- MacArther, A., Alonso, L., Malthus, T. & Moreno, J. (2013). Spectroscopy field strategies and their effect on measurements of heterogeneous and homogeneous Earth surfaces. In Proceedings of the 2013 Living Planet Symposium, Edinburgh, UK, 722 (December), 47. <https://ui.adsabs.harvard.edu/abs/2013ESASP.722E..47M/abstract>
- Malone, B. P., Styc, Q., Minasny, B., & McBratney, A. B. (2017). Digital soil mapping of soil carbon at the farm scale: A spatial downscaling approach in consideration of measured and uncertain data. *Geoderma*, 290, 91–99. <https://doi.org/10.1016/j.geoderma.2016.12.008>
- Meersmans, J., Van Wesemael, B., De Ridder, F., Dotti, M. F., De Baets, S., & Van Molle, M. (2009). Changes in organic carbon distribution with depth in agricultural soils in northern Belgium, 1960–2006. *Global Change Biology*, 15(11), 2739–2750. <https://doi.org/10.1111/j.1365-2486.2009.01855.x>
- Miklos, M., Short, M. G., McBratney, A. B., & Minasny, B. (2010). Mapping and comparing the distribution of soil carbon under cropping and grazing management practices in Narrabri, north-west New South Wales. *Australian Journal of Soil Research*, 48(3), 248–257. <https://doi.org/10.1071/SR09111>
- Mohamed, E. S., Saleh, A. M., Belal, A. B., & Gad, A. A. (2018). Application of near-infrared reflectance for quantitative assessment of soil properties. *Egyptian Journal of Remote Sensing and Space Science*, 21(1), 1–14. <https://doi.org/10.1016/j.ejrs.2017.02.001>
- Nocita, M., Stevens, A., van Wesemael, B., Aitkenhead, M., Bachmann, M., Barthès, B., ... Wetterlind, J. (2015). Soil spectroscopy: An alternative to wet chemistry for soil monitoring. *Advances in Agronomy*, 132, 139–159. <https://doi.org/10.1016/bs.agron.2015.02.002>
- Ontl, T. A., & Schulte, L. A. (2012). Soil carbon storage. *Soil Carbon Storage*, 3(10), 22–33.
- Robertson, G. P., Gross, K. L., Hamilton, S. K., Landis, D. A., Schmidt, T. M., Snapp, S. S., & Swinton, S. M. (2014). Farming for ecosystem services: An ecological approach to production agriculture. *Bioscience*, 64(5), 404–415. <https://doi.org/10.1093/biosci/biu037>
- Sarkhot, D. V., Grunwald, S., Ge, Y., & Morgan, C. L. S. (2011). Comparison and detection of total and available soil carbon fractions using visible/near infrared diffuse reflectance spectroscopy. *Geoderma*, 164 (1–2), 22–32. <https://doi.org/10.1016/j.geoderma.2011.05.006>
- Savitzky, A., & Golay, M. J. E. (1964). Smoothing and differentiation of data by simplified least squares procedures. *Analytical Chemistry*, 36(8), 1627–1639. <https://doi.org/10.1021/ac60214a047>
- Shi, P., Castaldi, F., van Wesemael, B., & Van Oost, K. (2020). Vis-NIR spectroscopic assessment of soil aggregate stability and aggregate size distribution in the Belgian Loam Belt. *Geoderma*, 357, 113958. <https://doi.org/10.1016/j.geoderma.2019.113958>
- Stenberg, B., Viscarra Rossel, R. A., Mouazen, A. M., & Wetterlind, J. (2010). Visible and near infrared spectroscopy in soil science. In *Advances in Agronomy* (Vol. 107, pp. 163–215). Amsterdam: Elsevier. [https://doi.org/10.1016/S0065-2113\(10\)07005-7](https://doi.org/10.1016/S0065-2113(10)07005-7)
- Stockmann, U., Adams, M. A., Crawford, J. W., Field, D. J., Henakaarchchi, N., Jenkins, M., Minasny, B., McBratney, A. B., Courcelles, V. . R. ., Singh, K., Wheeler, I., Abbott, L., Angers, D. A., Baldock, J., Bird, M., Brookes, P. C., Chenu, C., Jastrow, J. D., Lal, R., ... Zimmermann, M. (2013). The knowns, known unknowns and unknowns of sequestration of soil organic carbon. *Agriculture, Ecosystems and Environment*, 164, 80–99. <https://doi.org/10.1016/j.agee.2012.10.001>
- Vašát, R., Heuvelink, G. B. M., & Borůvka, L. (2010). Sampling design optimization for multivariate soil mapping. *Geoderma*, 155(3–4), 147–153. <https://doi.org/10.1016/j.geoderma.2009.07.005>
- Wu, C. Y., Jacobson, A. R., Laba, M., & Baveye, P. C. (2009). Accounting for surface roughness effects in the near-infrared reflectance sensing of soils. *Geoderma*, 152(1–2), 171–180. <https://doi.org/10.1016/j.geoderma.2009.06.002>
- Zhang, H., Aldana-Jague, E., Clapuyt, F., Wilken, F., Vanacker, V., & Van Oost, K. (2019). Evaluating the potential of post-processing kinematic (PPK) georeferencing for UAV-based structure-from-motion (SfM) photogrammetry and surface change detection. *Earth Surface Dynamics*, 7(3), 807–827. <https://doi.org/10.5194/esurf-7-807-2019>

**How to cite this article:** Zhang, H., Shi, P., Crucil, G., van Wesemael, B., Limbourg, Q., & Van Oost, K. (2021). Evaluating the capability of a UAV-borne spectrometer for soil organic carbon mapping in bare croplands. *Land Degradation & Development*, 1–15. <https://doi.org/10.1002/ldr.4043>

APPENDIX A

**TABLE A1** Performance of SOC prediction using SSL-based regional model on original UAV spectra and aligned UAV spectra

Dataset	RMSE (g kg <sup>-1</sup> )	R <sup>2</sup>	RPD	RPIQ
Original UAV-based spectra	3.43	0.34	0.35	0.39
Aligned UAV-based spectra	0.92	0.48	1.29	1.45



(b)

Dataset	Full bands				Selected bands			
	RMSE (g kg <sup>-1</sup> )	R <sup>2</sup>	RPD	RPIQ	RMSE (g kg <sup>-1</sup> )	R <sup>2</sup>	RPD	RPIQ
Laboratory	2.66	0.61	1.61	1.94	2.59	0.64	1.65	1.99
Proximal	2.32	0.71	1.84	2.20	2.19	0.74	1.94	2.32
UAV	0.89	0.52	1.38	1.56	0.72	0.67	1.73	1.95

**FIGURE A1** Results of the ensemble band-selection approach in SOC prediction in the three datasets. (a) Results of selected bands. Black and white color range in each graph illustrates the relative importance of the respective selected bands (in yellow) in each dataset. (b) Cross-validation results showing SOC prediction using the full bands and selected bands [Colour figure can be viewed at wileyonlinelibrary.com]

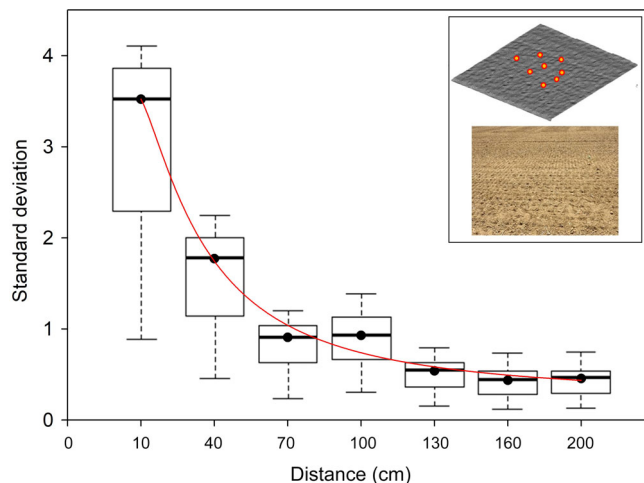


**FIGURE A2** Boxplot showing the standard deviation of spectra in Vis-NIR (400–1000 nm) regions measured at random positions at different heights [Colour figure can be viewed at wileyonlinelibrary.com]

**FIGURE A3** Flowchart showing the spectral alignment workflow for SSL-based SOC modelling and mapping

